

## Corrosion Resistance Investigation of Titanium Alloy as Tissue Engineered Bone Implant

Shengxin Zhou<sup>1#</sup>, Jin Wang<sup>2#</sup> and Pan Cai<sup>3\*</sup>

<sup>1</sup> The First Department of Orthopaedics, Pingyi County People's Hospital of Shandong, No.7 Jinhua Rd, Economic Development Area, Pingyi, Shandong, P.R. China

<sup>2</sup> Department of Joint orthopedic surgery, The First People's Hospital of Hefei, Anhui, P.R. China.

<sup>3</sup> Department of Orthopedics, Shanghai Zhoupu Hospital, Pudong New Area. 1500 Zhouyuan Rd, Zhoupu, Shanghai, 201318, P.R. China.

# These authors contributed equally in this work

\*E-mail: [pancai\\_163s@foxmail.com](mailto:pancai_163s@foxmail.com)

Received: 2 May 2017 / Accepted: 18 June 2017 / Published: 12 July 2017

---

This work used electrochemical impedance measurements and anodic polarisation to study the corrosion susceptibility of Ti, Ti-6Al-4V and TZNT in a buffered saline solution (PBS). The impedance characterization model was obtained under open-circuit conditions and was a double-oxide film model consisting of an inner-barrier oxide layer and a porous, outer layer. Low-pitting potentials were obtained for TZNT. The property of the outer layer depended on the presence of phosphate anions in the saline-buffered solution (SBS) and the electrode material. The typical, low resistances of the porous layers generated on TZNT with phosphate anions ranged from 10 to 70  $\Omega \text{ cm}^2$ . Ti, TZNT and Ti-6Al-4V all displayed much higher porous layer resistances without phosphate anions.

---

**Keywords:** Titanium alloy; Bone implant; Corrosion resistance; Electrochemical impedance spectroscopy; Medical application

### 1. INTRODUCTION

The need for rapid osseointegration and stability of titanium implants has increased [1-3]. To prevent micro-motion and ensure successful implantation (primarily for immediate loading), fast osseointegration and bone remodelling of the implant is necessary. The quantity and/or quality of bad bone requires higher stimulation to achieve rapid, new bone generation, which is similar to the case of patients suffering from severe ridge resorption. Orthopaedic implanting is another field that is interested in this issue [4-6]. A few synergistic and contemporary functions are needed to achieve a high osteointegration capacity, thus, a description of a multifunctional surface is presented herein. The

absence of infections, a high-degree of cell differentiation, fast adhesion and proliferation of osteoblastic cells, protein adsorption, the bioactivity of the surface and apatite precipitation (mineralization) cooperatively lead to rapid healing and new bone formation. Because fast osteointegration lowers the risk of infection, rapid bacteria proliferation is associated with slow osteointegration. A “race to the surface” after implantation using fast, osteoblast-induced implant colonization could prevent bacteria-involved colonization on the same surface [7, 8]. Based on recent research, biological functionalization could be used to obtain a specific biological response, and the modification and tailoring of the surface wettability, topography and chemistry could be used to create a multifunctional action surface [9-11]. In addition, a scientific study has also shown there is interest in the enhancement of the anti-corrosion and mechanical features of Ti-based materials [12, 13]. To enhance the bone-bonding ability of titanium-based implants, large numbers of solutions have been developed in the medical equipment market and in scientific works with the aim of enhancing the bone-bonding ability of titanium-based implants [14-18].

Titanium allotropically transforms from a hcp structure ( $\alpha$ -phase) to a bcc structure ( $\beta$ -phase) at a temperature of 882°C [19]. The titanium alloys were divided into three sub-types, including  $\alpha$  alloys,  $\beta$  alloys and  $\alpha+\beta$  alloys, due to this structural variation. The selected alloying additions were  $\alpha$  stabilizers, and the other elemental additions were  $\beta$  stabilizers. The corrosion of metal implants is importance since corrosion can have adverse effects on the mechanical integrity and biocompatibility of implants. The material used cannot lead to any adverse biological reactions in the body. In addition, the material should have stability and maintain its functional nature. Corrosion and surface film dissolution are different mechanisms that introduce additional ions into the body. Adverse biological reactions can be caused by excessive metal ion release, and the release results in the mechanical failure of the equipment. Amorphous titanium dioxide is the main constituent in the passive films produced on titanium and its alloys [20-22]. The electrochemical and physicochemical features of the oxide film and its long-term stability under biological circumstances determine the biocompatibility of titanium implants [23-26].

In this work, the effect of the alloy constituents and potential on the corrosion resistance of Ti, Ti-6Al-4V and Ti<sub>12.5</sub>Zr<sub>2.5</sub>Nb<sub>2.5</sub>Ta (TZNT) biomedical implant alloys was investigated using an electrochemical impedance spectroscopy (EIS) method under simulated physiological conditions. A surface-modified layer, created by H<sub>2</sub>O<sub>2</sub>-HNO<sub>3</sub>-containing polarization, was obtained. A higher corrosion resistance was observed. The passive film on the treated, commercially pure titanium surface was thinner and had a lower hydroxylation degree and reactivity than the film on the treated alloy.

## 2. EXPERIMENTS

Ti-6Al-4V, pure titanium (99.999%) and Ti<sub>12.5</sub>Zr<sub>2.5</sub>Nb<sub>2.5</sub>Ta (TZNT) were purchased from Tuteng Metal Co. Ltd. (Baoji, China) and used to prepare the electrodes. The electrode rods were embedded into an epoxy resin in a Teflon holder, and a copper wire was threaded into the metal specimen base to realize electrical contact. The TZNT wire electrodes were fabricated via polarization

in a  $\text{HNO}_3$ -containing solution with 0.1 M  $\text{H}_2\text{O}_2$ . This primary oxidation pretreatment for deliberate electrode fabrication eliminates the crevice attack that occurs at the interface of the resin and electrode. The exposed surfaces were polished to a smooth surface finish before each experiment. The auxiliary electrodes were high-density graphite rods. The reference electrode was a saturated calomel electrode (SCE), and all the potentials were recorded relative to the reference electrode. PBS was used as the electrolyte, and the solutions were kept at  $37^\circ\text{C}$  throughout the experiments.

Potentiodynamic electrochemical experiments were performed using a PARC 5210 lock-in amplifier-supported PARC 263 A potentiostat. The working electrodes were polarized below the corrosion potential of 30 mV in the anodic direction (scan rate: 0.5 mV/s) after an initial delay period (0.5 h) under open-circuit conditions. All the current data were obtained with respect to the geometric surface area. An EI 1287 electrochemical interface and a Solartron 1250 frequency response analyser were used to obtain the impedance measurement data. Spectra were obtained at the corrosion potential under open-circuit conditions for varied immersion times. The corrosion experiments were conducted at  $37 \pm 1^\circ\text{C}$  in Hank's SBF, and the composition is given in Table 1. All impedance data (real and imaginary components) were fitted to proper equivalent circuits using a complex, non-linear least-squares fitting procedure. The excitation voltage (10 mV) was applied throughout the experiments.

**Table 1.** Composition of Hank's simulated body fluid.

Regent	Amount (g/L)	Regent	Amount (g/L)
NaCl	8.00	$\text{C}_6\text{H}_6\text{O}_6$	1.00
KCl	0.40	$\text{MgCl}_2 \cdot 6\text{H}_2\text{O}$	0.10
$\text{CaCl}_2$	0.14	$\text{MgSO}_4 \cdot 7\text{H}_2\text{O}$	0.06
$\text{NaHCO}_3$	0.34	$\text{KH}_2\text{PO}_4 \cdot \text{H}_2\text{O}$	0.06
$\text{Na}_2\text{HPO}_4 \cdot 7\text{H}_2\text{O}$	0.05		

### 3. RESULTS AND DISCUSSION

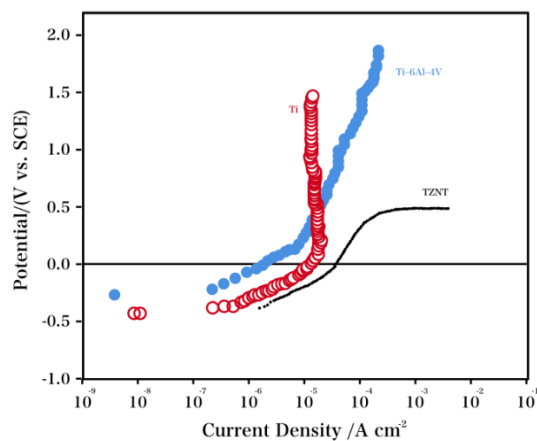


**Figure 1.** Anodic polarization curves of Ti, Ti-6Al-4V and TZNT in PBS at  $37^\circ\text{C}$ .

The anodic polarisation performances of Ti, TZNT and Ti–6Al–4V, which were polarized in PBS at 37°C, are characterized in Fig. 1 (Scan rate: 0.5 mV/s). The plots for Ti and Ti–6Al–4V are typical of significantly passive systems. In terms of the Ti electrode, the passive current density was  $2.5 \mu\text{A}/\text{cm}^2$ . The current remained low even when the potential was more anodic than 1.6 V. Compared with titanium polarized in Hank's solutions, the titanium in this work exhibited a higher passive current density. According to other studies [27-29], Ti and its alloys are composed of a double-layered oxide consisting of a porous, outer layer and an inner-barrier layer.

However, the higher density is because the scan rates used in this study were higher than the potentiostatic or typically used slow scan rates (0.15 mV/s). Ti–6Al–4V exhibited a similar performance, but the anodic current increased to ca.  $18 \mu\text{A}/\text{cm}^2$  at 1.0 V as the potential increased. Nevertheless, TZNT, the shape-memory alloy, showed a remarkably varied electrochemical performance. The potential oscillations during the polarization could be due to a balance between de-passivation and re-passivation on the wear tracks [30]. At comparatively low anodic potentials, a passive system, which was characterized by a low passive current density, was indicated. However, in the potential region of 0.2 V, an obvious, stable anodic current increase, which is typical of passive film breakdown and pitting attack, was observed.

Physiological media containing ions such as fluoride and chloride can break the oxide film that forms and cause pitting corrosion [31, 32]. Several pitting scans were performed to study the statistical property of the pitting attack on the TZNT electrode, and the pitting potential was calculated considering the cumulative possibility of the pitting occurrence. Fig. 2 shows the pitting potentials as a function of the cumulative possibility. The variation in the pitting potentials was observed in the range from 200 (comparatively low) to 520 mV, and the mean value was calculated to be 377 mV. The susceptibility of the TZNT electrode to a pitting attack was shown by these results.

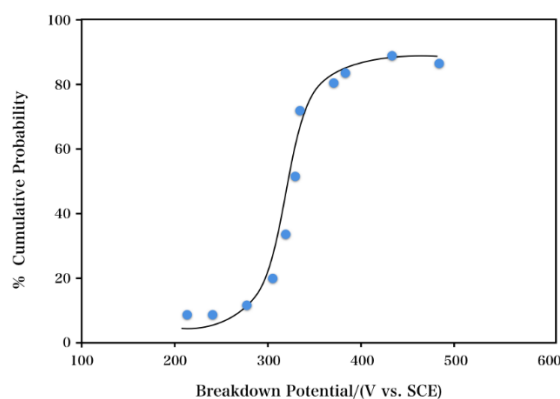


**Figure 2.** Cumulative probability plot of the breakdown potentials for TZNT in PBS at 37°C.

Fig. 3A indicates the characteristic cyclic polarisation data for TZNT in PBS at 37°C (scan rate: 1.0 mV/s), and the data suggested that, for the TZNT electrode, repassivation is unlikely upon its activation. A low passive current density (ca.  $1 \mu\text{A}/\text{cm}^2$ ) was obtained for the forward scan, which corresponded to the passive performance. The pitting attack initiation was indicated by the remarkable

increase in the current recorded ca. 570 mV. Upon polarization of the electrode, there is a temporary decrease in the current, which continued in the anodic direction. Studies have reported that the liberation of small amounts of alloy elements can cause cytotoxic effects in the human body and lead to adverse reactions when the alloy presents an elastic modulus that is incompatible with the bone. This incompatibility might cause a stress shield between the implant and the bone, which can cause bone resorption and premature failure in the implant [33, 34]. However, a repeated, rapid increase ca. 800 mV was observed. Upon an increase in the anodic current over  $1 \text{ mA/cm}^2$ , the applied potential was reversed and scanned in the electronegative direction. Nevertheless, the anodic current continued to increase to a density of ca.  $0.3 \text{ A/cm}^2$ , which indicated increasing pitting attack rates despite the decreased potential. Even at 0 V, a high anodic current was still observed, which suggested the absence of repassivation under these conditions.

The TZNT electrode resistance to pitting attack initiation was increased via surface modification. Fig. 3B displays the characteristic anodic polarisation plots for the Ti-45Ni electrode after it was modified. The electrode was immersed in a  $\text{H}_2\text{O}_2$  solution (100 mM) containing a supporting electrolyte,  $\text{Na}_2\text{SO}_4$  (0.1 M), and was polarized (open-circuit potential - 800 mV) to modify the surface. Three separate plots that are characteristic of the recorded data are displayed herein. As shown in these results, the breakdown potential remarkably increased after the surface modification process. The increase in the potential indicated that the sample possibly underwent an electrochemical reaction in the electrolyte medium, and a porous or defective oxide layer was formed. The passive region is associated with the formation of one or more protective oxide films. Compared with the unmodified electrodes, the modified electrodes regained their activity at low potentials upon activation.

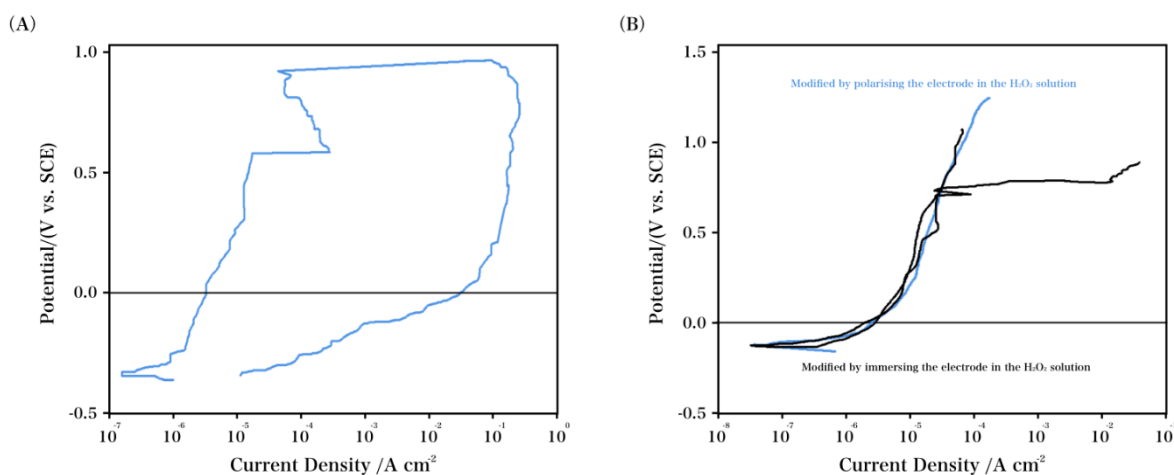


**Figure 3.** (A) Cyclic polarization plot for TZNT in PBS at  $37^\circ\text{C}$ . (B) Anodic polarization plots for TZNT in PBS at  $37^\circ\text{C}$  after modification in a solution containing  $\text{H}_2\text{O}_2$ .

The characteristic electrochemical impedance data for Ti in PBS at  $37^\circ\text{C}$  under open-circuit conditions after 300 and 1000 min of immersion are displayed in Fig. 4A. According to the impedance data, the Ti system has a capacitive performance over a comparatively wide frequency domain, which

is characteristic of passive systems. There was a time-related evolution for the impedance response, as shown in the comparison of the two sets of test data. The high frequency and medium frequency domains both showed almost no variations in their patterns, while the lower frequency domain exhibited a remarkable variation. The plots in Fig. 4B show that the fitting parameters changed with the immersion time. The resistance elements are displayed as a function of time (Fig. 4B), and the constant phase elements as a function of time are shown in a similar plot (Fig. 4C). During the 900-min immersion, the resistance element,  $R_{pr}$ , was essentially stable. However, as the immersion time lengthened, there is an element,  $R_1$ , increase that represents the barrier layer resistance, which indicated a reduction in the corrosion resistance of the samples.

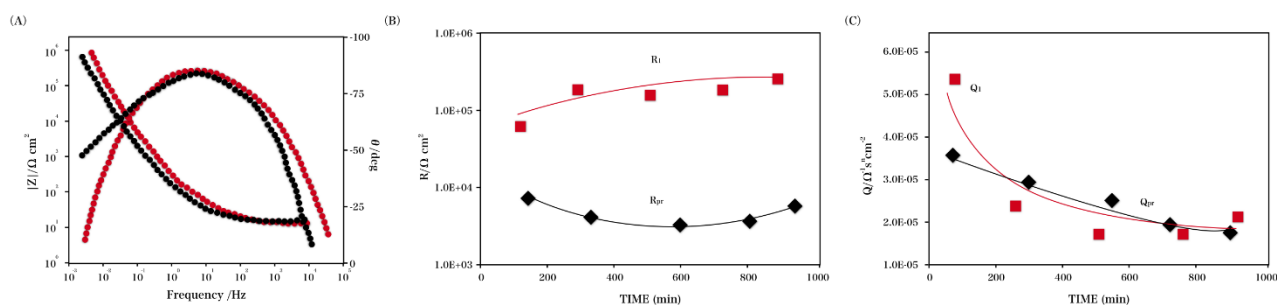


**Figure 4.** (A) Impedance data for Ti in PBS at 37°C. (B) Resistance elements and (C) constant phase elements plotted as a function of time for Ti in PBS at 37°C.

The Ti-6Al-4V alloy in PBS at 37°C under open-circuit conditions after 120 and 1000 min immersions was characterized via a characteristic electrochemical impedance spectrum, as shown in Fig. 5A. The experimental data also agrees well with the simulated data. Fig. 5B shows a Nyquist plot of the impedance data, and the data indicated that a diffusion element exists. The low-frequency data are represented by a line at an angle of 45°, which suggested diffusion processes across the double-oxide layer on the implant electrode. The property variation in the Ti-6Al-4V passive layer depends on the time, as indicated by the two plots (Fig. 5A). The near capacitive performance in the mid-frequency domain is characteristic of the impedance response during the early stages of immersion, and the diffusion processes are obvious at low frequencies. The resistance elements,  $R_{pr}$  and  $R_1$ , are displayed in Fig. 5C, and the constant phase elements,  $Q_{pr}$ ,  $Q_1$  and  $Q_2$ , are displayed in Fig. 5D. Both elements are displayed as a function of the immersion period for Ti-6Al-4V in PBS.  $R_{pr}$  was below  $5 \Omega \cdot \text{cm}^2$  during the early stages of immersion and increased to  $30 \Omega \cdot \text{cm}^2$ . A film that has a high resistance should have a high corrosion resistance, and a decrease in the passive film capacitance correlates with the slow growth of the titanium and molybdenum oxides and the long-term stability of the thin passive film [35-37]. The aforementioned values display an extremely low resistance for the porous layer. In comparison,  $R_1$ , which represents the inner-barrier layer resistance, had a high value in all the analyses. With an increase in the  $R_{pr}$  term, the constant phase element of  $Q_{pr}$  decreased during the early immersion stage.  $Q_1$  was basically steady in all the tests, which suggested the inner-barrier passive film is stable, but there was a slight increase in the diffusion component with the immersion time.

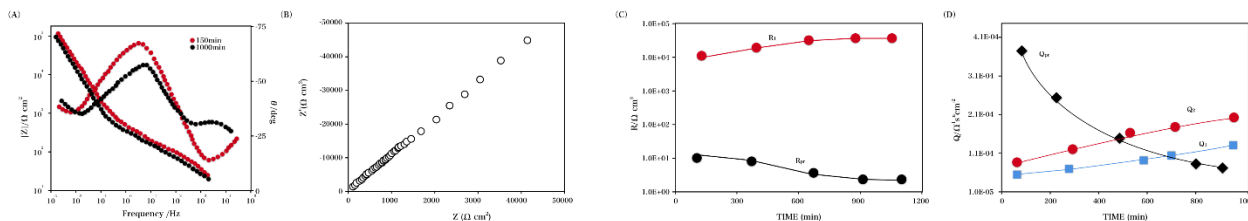


**Figure 5.** (A) Impedance data for Ti-6Al-4V in PBS at 37°C. (B) Nyquist plot of Ti-6Al-4V after 1000 min. (C) Resistance elements and (D) constant phase elements plotted as a function of time for Ti-6Al-4V in PBS at 37°C.

Fig. 6 shows similar impedance data for TZNT in the phosphate buffered chloride solution. The plot recorded after 1 h of immersion in the saline solution is represented by the symbols, and the corresponding simulated data are represented by the solid lines. The experimental data agreed with the simulated data. These results corresponded to the results of the TZNT system. Specifically, the impedance response is characteristic of a diffusion element dominating the response in the low-frequency domain, and a near capacitive element dominates the response in the medium-frequency domain during the early stage immersion. Nevertheless, a high-frequency term forms after constant immersion. Fig. 6B and 6C display the equivalent circuit parameters ( $R_{pr}$  and  $R_1$ ) and the constant phase elements ( $Q_{pr}$ ,  $Q_1$  and  $Q_2$ ), respectively, for TZNT as a function of the immersion period. There was an increase in  $R_{pr}$  (below  $10 \Omega \text{ cm}^2$  – ca.  $70 \Omega \text{ cm}^2$ ) for Ti-6Al-4V as the immersion continued. However, the parameters indicated comparatively low resistances.  $Q_{pr}$  represents the initial, outer, porous layer drop and reached a steady-state value after a short period of time.  $Q_1$  represents the capacitance of the inner passive film and was constant throughout the experiments.  $R_1$  remained constant at values of approximately  $4.0 \times 10^4 \Omega \text{ cm}^2$ , which suggested stable passive conditions. Although this indicated the stability of the TZNT system, the slight increase in the diffusion term  $Q_2$  was confirmed after immersion for over 2000 min.

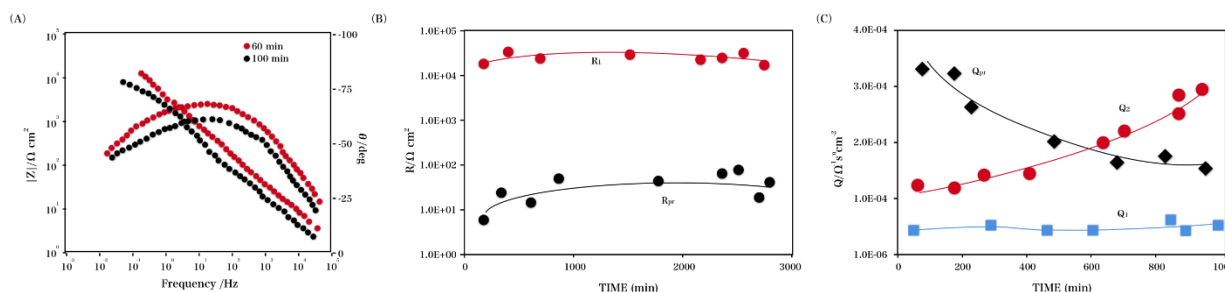


**Figure 6.** (A) Impedance data for TZNT in PBS at 37°C. (B) Resistance elements and (C) constant phase elements plotted as a function of time for TZNT in PBS at 37°C.

#### 4. CONCLUSIONS

This study investigated the corrosion resistance of TZNT, Ti and Ti-6Al-4V in a saline-buffered solution. As shown in the results, Ti and Ti-6Al-4V displayed high resistances to the

initiation of localized corrosion, but the initiation of pits occurred at low potentials on TZNT. TZNT exhibited an increasing number of noble pitting potentials during surface modification in a H<sub>2</sub>O<sub>2</sub>-containing solution. Nevertheless, TZNT before and after modification displayed low repassivation potentials, which suggested that upon initiation, the pits could propagate at potentials remarkably lower than the pitting potential. The passive films produced on the aforementioned electrodes were assayed with respect to a double-oxide layer, which consisted of an outer, porous layer and an inner barrier. The properties of the porous layer are dependent on the features of the alloy and the solution anion groups.

#### ACKNOWLEDGEMENT

This work was supported by Shanghai Medical Specialist Fund (ZK2015A14).

#### References

1. M. Chiapasco, P. Casentini and M. Zaniboni, *International Journal of Oral & Maxillofacial Implants*, 24 (2009)
2. D. Paquette, N. Brodala and R. Williams, *Dental Clinics of North America*, 50 (2006) 361.
3. Y. Manor, S. Oubaid, O. Mardinger, G. Chaushu and J. Nissan, *Journal of Oral and Maxillofacial Surgery*, 67 (2009) 2649.
4. S. Bauer, P. Schmuki, K. von der Mark and J. Park, *Progress in Materials Science*, 58 (2013) 261.
5. M. Geetha, A. Singh, R. Asokamani and A. Gogia, *Progress in Materials Science*, 54 (2009) 397.
6. D. Ehrenfest, P. Coelho, B. Kang, Y. Sul and T. Albrektsson, *Trends Biotechnol.*, 28 (2010) 198.
7. A. Gristina, P. Naylor and Q. Myrvik, Biomaterial-centered infections: microbial adhesion versus tissue integration, *Pathogenesis of Wound and Biomaterial-Associated Infections*, Springer1990, pp. 193.
8. L. Harris and R. Richards, *Injury*, 37 (2006) S3.
9. A. Elkarargy, *International Journal of Health Sciences*, 8 (2014) 57.
10. G. Ahmed, *Journal of American Science*, 9 (2013)
11. C. Chien and W. Tsai, *ACS Appl. Mater. Interfaces*, 5 (2013) 6975.
12. X. Ye, L. Wang, T. Zion, G. Tang and G. Song, *Materials Science and Engineering: C*, 49 (2015) 851.
13. X. Ye, T. Zion, G. Tang and G. Song, *Journal of the Mechanical Behavior of Biomedical Materials*, 42 (2015) 100.
14. G. Zhao, A.L. Raines, M. Wieland, Z. Schwartz and B. Boyan, *Biomaterials*, 28 (2007) 2821.
15. C. Schmidt, D. Kaspar, M. Sarkar, L. Claes and A. Ignatius, *J. Biomed. Mater. Res., Part A.*, 63 (2002) 252.
16. A. Zareidoost, M. Yousefpour, B. Ghaseme and A. Amanzadeh, *J. Mater. Sci.: Mater. Med.*, 23 (2012) 1479.
17. F. Variola, J.B. Brunski, G. Orsini, P.T. de Oliveira, R. Wazen and A. Nanci, *Nanoscale*, 3 (2011) 335.
18. F. Vetrone, F. Variola, P. Tambasco de Oliveira, S.F. Zalzal, J.-H. Yi, J. Sam, K.F. Bombonato-Prado, A. Sarkissian, D. Perepichka and J. Wuest, *Nano Lett.*, 9 (2009) 659.
19. J. González and J. Mirza-Rosca, *J. Electroanal. Chem.*, 471 (1999) 109.
20. E. Vasilescu, P. Drob, D. Raducanu, V. Cojocar, I. Cinca, D. Iordachescu, R. Ion, M. Popa and C. Vasilescu, *J. Mater. Sci.: Mater. Med.*, 21 (2010) 1959.
21. C. Fleck and D. Eifler, *International Journal of Fatigue*, 32 (2010) 929.

22. J. Li, L. Zhou and Z. Li, *Rare Metals*, 29 (2010) 37.
23. Y. Huang, X. Zhang, H. Qiao, M. Hao, H. Zhang, Z. Xu, X. Zhang, X. Pang and H. Lin, *Ceram. Int.*, 42 (2016) 1903.
24. Y. Huang, H. Zeng, X. Wang and D. Wang, *Appl. Surf. Sci.*, 290 (2014) 353.
25. E. Vasilescu, P. Drob, I. Cinca, M. Popa and C. Vasilescu, *Revista De Chimie*, (2010) 0034.
26. J. Izquierdo, M. González-Marrero, M. Bozorg, B. Fernández-Pérez, H. Vasconcelos, J. Santana and R. Souto, *Electrochim. Acta*, 203 (2016) 366.
27. I. Park, T. Woo, M. Lee, S. Ahn, M. Park, T. Bae and K. Seol, *Metals and Materials International*, 12 (2006) 505.
28. S. Fadel-Allah, R. El-Sherief and W. Badawy, *J. Appl. Electrochem.*, 38 (2008) 1459.
29. Y. Pan, C. Chen, D. Wang and Z. Lin, *Mater. Chem. Phys.*, 141 (2013) 842.
30. M. Golozar, K. Raeissi and M. Fazel, *Surf. Coat. Technol.*, 244 (2014) 29.
31. S. Kumar and T. Narayanan, *Journal of Dentistry*, 36 (2008) 500.
32. N. Oliveira and A. Guastaldi, *Acta Biomaterialia*, 5 (2009) 399.
33. A. Tavares, B. Fernandes, S. Souza, W. Batista, F. Cunha, R. Landers and M. Macedo, *J. Alloy. Compd.*, 591 (2014) 91.
34. D. Martins, M. Souza, S. Souza, D. Andrade, C. Freire and R. Caram, *J. Alloy. Compd.*, 478 (2009) 111.
35. D. Mareci, R. Chelariu, D. Gordin, G. Ungureanu and T. Gloriant, *Acta Biomaterialia*, 5 (2009) 3625.
36. J. Gonzalez and J. Mirza-Rosca, *J. Electroanal. Chem.*, 471 (1999) 109.
37. A. Al-Mayouf, A. Al-Swayih, N. Al-Mobarak and A. Al-Jabab, *Mater. Corros.*, 55 (2004) 524.
38. K. Hou, C. Lin, C. Chen, B. Wu, D. Zhu, W. Zhong, X. Wang, X. Xie, Q. Chen. *Biomedical Research-India*, 28 (2017) 129.